

Reactivity of water vapor in an atmospheric argon flowing post-discharge plasma torch

S Collette, Thierry Dufour, F. Reniers

▶ **To cite this version:**

S Collette, Thierry Dufour, F. Reniers. Reactivity of water vapor in an atmospheric argon flowing post-discharge plasma torch. Plasma Sources Science and Technology, 2016, 25 (2), pp.025014. 10.1088/0963-0252/25/2/025014 . hal-01367339v3

HAL Id: hal-01367339

https://hal.sorbonne-universite.fr/hal-01367339v3

Submitted on 6 Mar 2023

HAL is a multi-disciplinary open access archive for the deposit and dissemination of scientific research documents, whether they are published or not. The documents may come from teaching and research institutions in France or abroad, or from public or private research centers.

L'archive ouverte pluridisciplinaire **HAL**, est destinée au dépôt et à la diffusion de documents scientifiques de niveau recherche, publiés ou non, émanant des établissements d'enseignement et de recherche français ou étrangers, des laboratoires publics ou privés.

This document is an author-edited version of the original article while presenting identical scientific content.

Title	**Reactivity of water vapor in an atmospheric argon flowing post-discharge plasma torch**
Authors	S Collette[1], T Dufour[1,2] and F Reniers[1]
Affiliations	[1] Faculté des Sciences, Service de Chimie Analytique et de chimie des Interfaces, Université Libre de Bruxelles, CP-255, Bld du Triomphe, B-1050 Bruxelles, Belgium [2] Sorbonne Université, Campus Pierre et Marie curie, 4 place Jussieu, 75005 Paris, France
Ref.	Plasma Sources Sci. Technol. 25 (2016) 025014 (11pp)
DOI	http://doi.org/10.1088/0963-0252/25/2/025014
Abstract	The reactivity of water vapor introduced in the flowing post-discharge of an RF atmospheric plasma torch is investigated through electrical characterization, optical emission spectroscopy and mass spectrometry measurements. Due to the technical features of the plasma torch, the post-discharge can be considered as divided into two regions: an inner region (inside the plasma torch device) where the water vapor is injected and an outer region which directly interacts with the ambient air. The main reactions induced by the injection of water vapor are identified as well as those indicative of the influence of the ambient air. Plausible pathways allowing the production of H, OH, O radicals and H_2O_2 are discussed as well as reactions potentially responsible for inhomogeneities and for a low DC current measured in the flowing post-discharge. Keywords: atmospheric post-discharge, H_2O plasma reactivity, RF plasma torch

I. Introduction

At first inspection, traces of water vapor in a plasma source may be considered as problematic since they can induce undesired chemical reactions [1, 2] and often instabilities [3]. However, for specific applications, water vapor can be deliberately mixed with the plasmagen gas either to achieve a milder treatment or to generate radicals of interest. This approach has already been investigated in various domains such as surface treatments [4], biocompatibility [5] or plasma medicine [6].

In surface treatments, the oxidative functionalization is usually achieved with O_2 [7–11]. This reactive gas can, however, be replaced by water vapor and mixed with a carrier gas to induce a milder treatment. For instance, the exposure of graphene to a pure oxygen plasma at 0.3 mbar leads to an over-etching of the top sheets even on short exposure times (few seconds) while the addition of water-vapor to the plasma allows a milder and more homogeneous treatment [12]. In any case, the presence of water vapor makes useless the utilization of a mask to filter the free radicals [12]. Another example deals with the oxidative functionalization of polypropylene: replacing O_2 by water vapor ensures a more homogeneous distribution of the alcohol, carbonyl and carboxyl groups on the surface, but also a functionalization achieved on a larger depth [4].

In biocompatibility applications, the functionalization of hydroxyl groups on polyethylene and polystyrene surfaces has achieved minor success by using either a pure O_2 plasma treatment or an Ar plasma treatment followed by an oxygen environment [13, 14]. Water plasma treatment could be considered as an alternative for the preparation of hydroxyl surfaces allowing the covalent immobilization of biologically active molecules and the support of cells colonization [5]. It could also be used for blood compatibility of PTFE prosthesis. For instance, König et al have followed a 3-step process [15] in which a water vapor microwave plasma is used as the first step to facilitate the subsequent post-grafting of acrylic acid on the PTFE surface (2nd step) and the immobilization of the fibrinolytic protein urokinase (3rd step).

In plasma medicine, the role of radicals, such as O, O_3, NO and OH, as well as ultraviolet radiation, are still under study for therapeutic applications such as wound healing or dermatology and tumor treatments [6]. For instance, Zhang et al showed the role of O, OH and Ar* radicals on the destruction of cancerous hepatocellular carcimona cells [16]. In this respect, water vapor could be used as a process gas to generate large densities of O and OH radicals.

All these applications clearly indicate that there are two requirements: Firstly, there is need for the understanding of the chemical mechanisms induced by water vapor at atmospheric pressure and, secondly, for a more specific control of the production of radicals. In this respect, an experimental study is presented in this article where the introduction of water vapor within the post-discharge of an Ar plasma torch is discussed in terms of plasma stability, chemical kinetics and radicals of interest. The results of the present study complement two previous studies published using the same plasma source, namely an experimental investigation by Duluard et al [17] and simulations from Atanasova et al [18].

II. Experimental methods

Figure 1 introduces a schematic diagram of the experimental setup, including the plasma source and a water-containing bubbler (at room temperature) dedicated to the injection of water vapor in the post-discharge. The plasma source is an atmospheric RF plasma torch from Surfx Technologies LLC (Atomflo™ 250D), consisting of two parallel circular electrodes perforated by 126 holes, each one with a critical diameter of 0.6 mm. A 126-holes circular metallic mesh is located parallel and downstream to the two electrodes to homogenize the flowing post-discharge. The gas flow is oriented perpendicularly to the two electrodes. As these

holes are arranged to form a circular pattern of 20 mm in diameter, this torch is commonly called a 'showerhead plasma torch'. For all the results discussed in the present article, it operates at a frequency of 27.12 MHz and a power fixed at 80 W. As sketched in figure 1, three regions can be distinguished: (i) the plasma region located between the RF and the ground electrodes, (ii) the inner post-discharge located between the ground electrode and the grid and (iii) the outer post-discharge located beyond the grid.

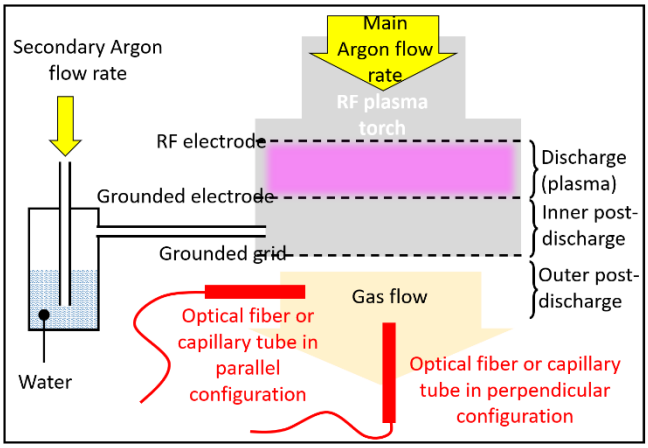


Figure 1. Schematic diagram of the experimental setup and location of the three discharge regions.

Two argon inputs were considered: the first one supplies the plasma torch for a flow rate of 30 L.min^{-1}; it is referenced here as the 'main Ar flow rate'. A second input—assigned here as the 'secondary Ar flow rate', supplies the bubbler via a volumetric flowmeter from Aalborg for flow rates comprised between 0 L min^{-1} and 6 L min^{-1}. An Ar/H_2O vapor mixture can therefore be generated and reach the inner post-discharge region via the plasma torch nozzle. Secondary (2nd) Ar flow rates of 0, 2, 4 and 6 L.min^{-1} correspond to H_2O flow rates of 0, 0.7, 1.3 and 2 mL.s^{-1}.

Optical emission spectroscopy (OES) was performed with a Spectra Pro-2500i spectrometer from ACTON research Corporation (0.500 m focal length, triple grating imaging). The light emitted by the post-discharge is collected by an optical fiber set either in a perpendicular configuration or a parallel configuration, as sketched in figure 1. The perpendicular configuration supplies only information on the outer post-discharge, whereas the parallel configuration gives information on the whole post-discharge (inner and outer). The light is then transmitted to the entrance slit (50 µm) of the monochromator where it is collimated, diffracted, focused on the exit slit and finally captured by a CCD camera from Princeton Instruments. Each optical emission spectrum is acquired with an 1800 grooves mm^{-1} grating (blazed at 500 nm) and recorded on 30 accumulations with an exposure time of 25 ms. Experimentally, we have observed that an increase in the H_2O flow rate has always induced a decrease in all the emission lines/bands of the post-discharge. As a consequence, from one water flow rate to another, the de-excitation of a specific species is always proportional to the overall decay of the post-discharge emission. To solve this problem, for every H_2O flow rate, the emissions of all the species were divided by the emission of the whole post-discharge (i.e. a continuum from 250 to 850 nm).

Mass spectra of the post-discharge were acquired with a quadripolar mass spectrometer (Balzers QMS 200) coupled with a turbo molecular pump (Pfeiffer TSU 062H) at a base pressure of approximately 1·10^{-8} mbar. The mass spectrometer measures the gaseous species in the post-discharge through a capillary tube, set either perpendicular or parallel to the gas flow. The capillary tube is 1 m in length, with an inner diameter of 0.1 mm. It is heated by a resistance to maintain the gas temperature at 150°C, thereby avoiding condensation before entering the ionization chamber. The ionization energy is set to 70 eV.

DC currents were measured in the post-discharge by placing a copper plate downstream. The distance separating the plasma torch from the copper plate is called the 'gap'. The current is obtained by measuring the voltage difference across a resistor (820 kOhm) connecting the copper plate to an oscilloscope. A digital phosphor oscilloscope from Tektronix (DPO3032) has been used, with a band gap of 300 MHz and a sample rate as high as 2.5 GS.s^{-1} for an accurate representation of the signals.

III. Results

Figure 2 introduces pictures of the post-discharge operating at an RF power of 80 W, supplied with a main argon flow rate fixed at 30 L.min^{-1} and a secondary (2nd) Ar flow rate set to either 2 L.min^{-1} or 6 L min^{-1} (with and without water in the bubbler). The amount of H_2O injected in the post-discharge is controlled by the secondary Ar flow rate. If no water is contained in the bubbler, the post-discharge emission is uniform and stable in each hole, whatever the secondary Ar flow rate. However, once water is introduced into the bubbler and carried under vapor via the secondary argon flow rate, the whole emission of the post-discharge vanishes and becomes inhomogeneous through the various holes, randomly changing as a function of time. Moreover, these inhomogeneities become stronger as the amount of water vapor carried by the secondary argon flow rate is increased. Therefore, the inhomogeneities of the post-discharge clearly result from the injected water vapor and not from the secondary Ar flow rate.

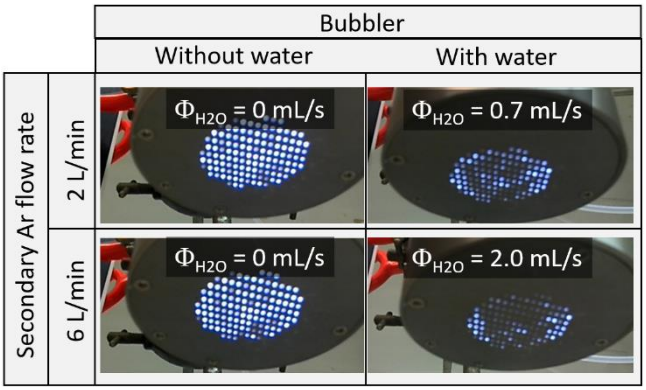


Figure 2. Influence of the water vapor and secondary Ar flow rates on the apparent post-discharge stability, for P=80 W, Φ(Ar) = 30 L.min^{-1}.

S Collette, T Dufour, F Reniers, Plasma Sources Sci. Technol. 25 (2016) 025014, http://doi.org/10.1088/0963-0252/25/2/025014

The influence of the H_2O flow rate on the post-discharge's electrical properties was carried out as described in the experimental methods. The post-discharge current as a function of the H_2O flow rate is represented in figure 3. Although some tentative interpretation of this current is given further in this paper (see 'stability' section in the discussion part), and although such current has already been observed and discussed in other papers (but for a torch fed with Helium) [19], these current measurements should only be taken here as qualitative data, hence showing a clear water-depending trend. Its variation shows a strong decrease between 0 and 0.7 mL.s^{-1} followed by a slower decay. Without water vapor, the post-discharge is stable, and a current of 32 µA is collected on the copper plate. For Φ_{H2O} = 2.7 mL.s^{-1}, a post-discharge current of only 4 µA is measured and corresponds to a lower-emissive and more inhomogeneous post-discharge, as shown in inset. This decrease in the post-discharge current is directly connected to the number of holes ignited in the post-discharge: they are 126 (maximum) without water vapour and less than 50 for Φ_{H2O} = 2.7 mL.s^{-1}.

Species	λ (nm)	Transition	Ref.
OH	309.1	$A^2\Sigma^+ \rightarrow X^2\Pi$	[20, 21]
O(^{5}P)	777.4	$2s^2 2p^3\left(\,^4S^0\right)3p \rightarrow 2s^2 2p^3\left(\,^4S^0\right)3s$	[20, 21]
N_2	337.1	$C^3\Pi_u \rightarrow B^3\Pi_g$	[20, 21]
Ar (^{3}P$_2$)	763.5	$3s^2 3p^5 4p \rightarrow 3s^2 3p^5 4s$	[20, 21]
H_α	656.3	$3\mathrm{d}\left(\,^2D\right) \rightarrow 2p\left(\,^2P^0\right)$	[22]

Table 1. Species detected by OES.

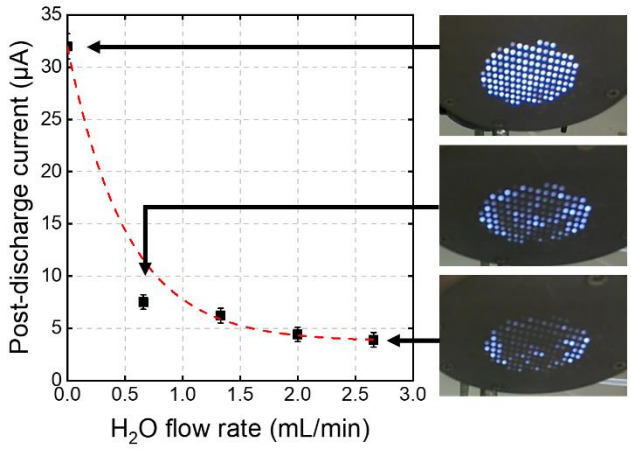


Figure 3. Influence of the H_2O flow rate on the post-discharge current. Gap = 10 mm. Ar flow rate = 30 L.min^{-1}, RF power = 80 W.

The influence of the H_2O flow rate was investigated by measuring the optical emission of several species reported in table 1 namely OH, O, N_2 and Ar for the plasma torch supplied with a power of 80 W and an Ar flow rate of 30 L.min^{-1}. Their variations were plotted as a function of the water flow rate in the perpendicular (figures 4(a) and (c)) and parallel configurations (figures 4(b) and (d)), considering either the influence of the secondary argon flow rate with water vapor (figures 4(a) and (b)) or only the influence of the water vapor (figures 4(c) and (d)) based on the relation $\varepsilon_{dif}\{H_2O\} = \varepsilon\{2^{nd}\ Ar+H_2O\} - \varepsilon\{2^{nd}\ Ar\}$ where ε stands for the emission and ε_{dif} the differential emission. Several observations are noteworthy:
(i) The comparison between figures 4(a) and (b) shows that stronger emissions are obtained in the perpendicular configuration with variations in emission of almost an order of magnitude between 0 and 2.7 mL.s^{-1}, except for Ar. In this configuration, the production of the OH species seems counterbalanced by the consumption of N_2 and O species. Similar trends appear also in the parallel configuration, albeit less significant.

(ii) Figures 4(c) and (d) indicate whether the presence of water vapor in the post-discharge enhances or not the differential emission of the species. If a species differential emission is positive ($\varepsilon_{dif} > 0$), then its density can be considered as more important than in a pure Ar post-discharge (such as OH in the perpendicular configuration). On the contrary, if a species differential emission is negative ($\varepsilon_{dif} < 0$), then its density is higher in the pure Ar post-discharge, such as O, N_2 and Ar species in the perpendicular configuration. Figures 4(c) and (d) also indicate whether the injection of water vapor enhances the reactions of production (if $|\varepsilon_{dif}|$ increases versus $\Phi(H_2O)$) or the reactions of consumption (if $|\varepsilon_{dif}|$ decreases with $\Phi(H_2O)$). As an example, in the parallel configuration, a rise in $\Phi(H_2O)$ increases the differential emission of the Ar line, thus indicating an increase in the density of these excited species.

(iii) The comparison between the {2nd Ar + H_2O} and {H_2O} cases (i.e. comparison between figures 4(a) and (c) or between (b) and (d)) indicates curves with consistent trends. As an example, in the parallel configuration for $\Phi(H_2O)$ = 0–2.7 mL.s^{-1}, the emission of O decreases from 800 to 250 a.u. in figure 4(a) while from 0 to −330 a.u. in figure 4(c). The reactivity of the emissive species is therefore much stronger in presence of water vapor.

(iv) Fourthly, whatever the graph shown in figure 4, the most significant variations in emission appear when the post-discharge passes from $\Phi(H_2O)$ = 0 to the tiniest injected flow rate. In figure 4(a), the emission of OH increases from 300 to 1350 a.u. for $\Phi(H_2O)$ comprised between 0 and 0.7 mL.s^{-1} while in figure 4(c), it increases from 0 to 980 a.u. for $\Phi(H_2O)$ = 0–2.7 mL.s^{-1}. For higher water flow rates, further variations in intensity are still visible although less significant, as if a plateau was reached (e.g. from 990 to 940 a.u. in the case of OH in figure 4(c)).

(v) A Hα line (656.3 nm) is solely observed in the parallel configuration. Its emission is particularly weak in presence of water vapor, even if it tends to slightly rise by increasing its flow rate.

This OES study was completed by taking measurements of the mass spectrometry. The following species were detected where the values in parentheses indicate their corresponding m/z ratios: H (1), H_2 (2), N (14), O (16), OH (17), H_2O (18), N_2 (28), O_2 (32), H_2O_2 (34) and Ar (40). The intensity of the species previously detected by OES (OH, O, N_2, Ar and H) are plotted in figure 5 and the intensity of the others in figure 6 versus the H_2O flow rate. As in the OES results, each figure comprises four graphs where the

perpendicular configuration (a&c), the parallel configuration (b&d), the influence of {2nd Ar + H_2O} (a&b) and the influence of {H_2O} (c&d) are considered. The aforementioned observations still apply with respect to figure 5: the MS intensities are stronger in the perpendicular configuration, and similar MS intensities trends are obtained between the {2nd Ar + H_2O} and {H_2O} cases but not necessarily between the ⊥ and // configurations. The most significant variations in emission were detected from 0 to the tiniest measured Φ(H_2O) flow rate. As in the OES results, the presence of water vapor increases the intensities of OH whilst reducing the intensities of O and N_2, whatever the configuration. Furthermore, in the MS results as in the previous OES results, an increase in Φ(H_2O) induces a lowering of the Ar intensity in the ⊥ configuration while a rising in the // configuration. In figure 6, where species resulting from non-radiative processes are reported, an increase in Φ(H_2O) indicates a strong increase of both H_2O and O_2, a slight increase of both H_2O_2 and H_2 and, finally, a decrease in N, whatever the configuration.

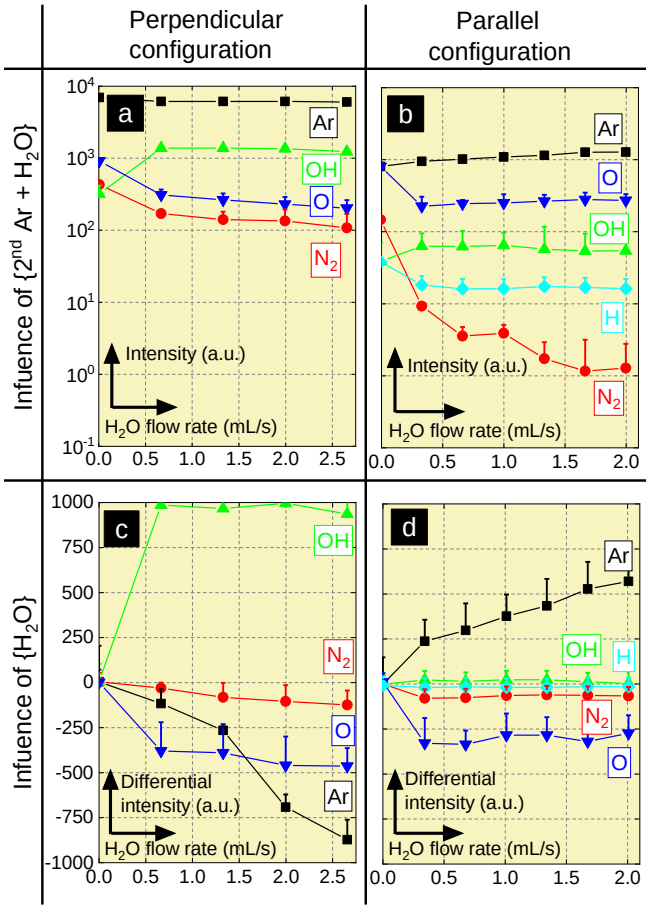


Figure 4. OES measurements showing the effect of the H_2O flow rate on the emission and differential emission of OH, O, N_2, Ar and H species (Ar flow rate = 30 L min^{-1}, power = 80 W). The differential emission is given by ε_{dif}{H_2O} = ε{2nd Ar + H_2O} – ε{2nd Ar}

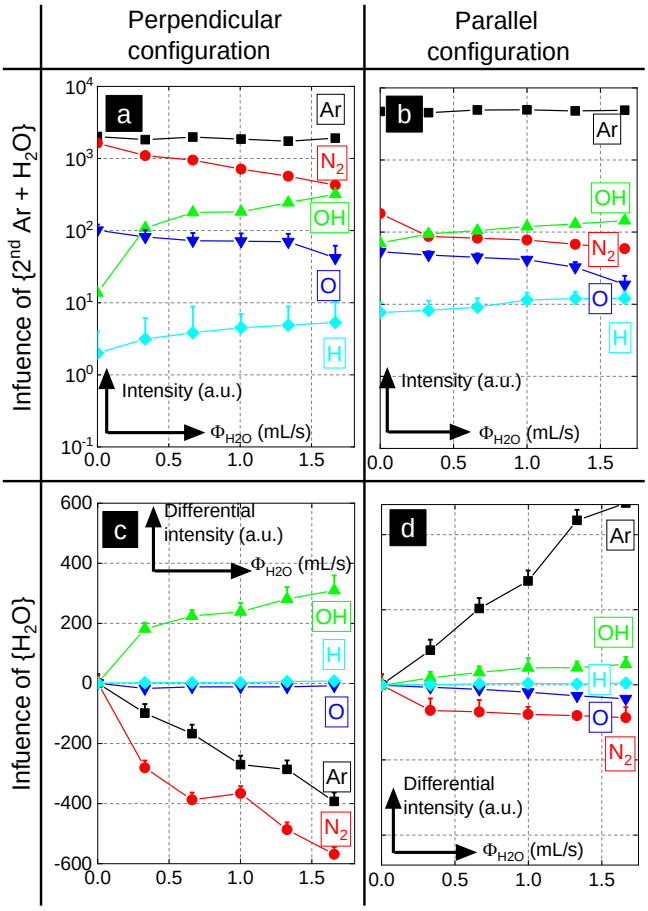


Figure 5. Mass spectrometry measurements showing the effect of the H_2O flow rate on the intensity and differential intensity of OH, O, N_2, Ar and H species (Ar flow rate = 30 L.min^{-1}, power = 80 W).

IV. Discussion

The discussion is focused on the possible reactions occurring in the interelectrode and post-discharge regions for each species detected by OES and/or mass spectrometry. The stability of the post-discharge depending on the water vapor injected is also discussed.

IV.1. Ar species in the interelectrode region

In the interelectrode region, the production of non-ionized excited Ar species is expected through elementary processes such as elastic scattering [R-1], excitation [R-2] and recombination [R-3] (all the R-X reactions are described in table 2). The production of Ar^+ ions is achieved through the direct ionization reaction [R-4], as well as the stepwise ionization, described by reaction [R-5] and the Penning ionization resulting from the collision of two excited Ar atoms [R-6]. Besides this, the production of Ar_2^+ ions is also expected in the interelectrode region through the reactions [R-7], as supported by the simulations of Atanasova et al [18]. The production of Ar metastable species has also been evidenced through either electron collision [R-8] and Ar^+ collision [R-9] with Ar [23].

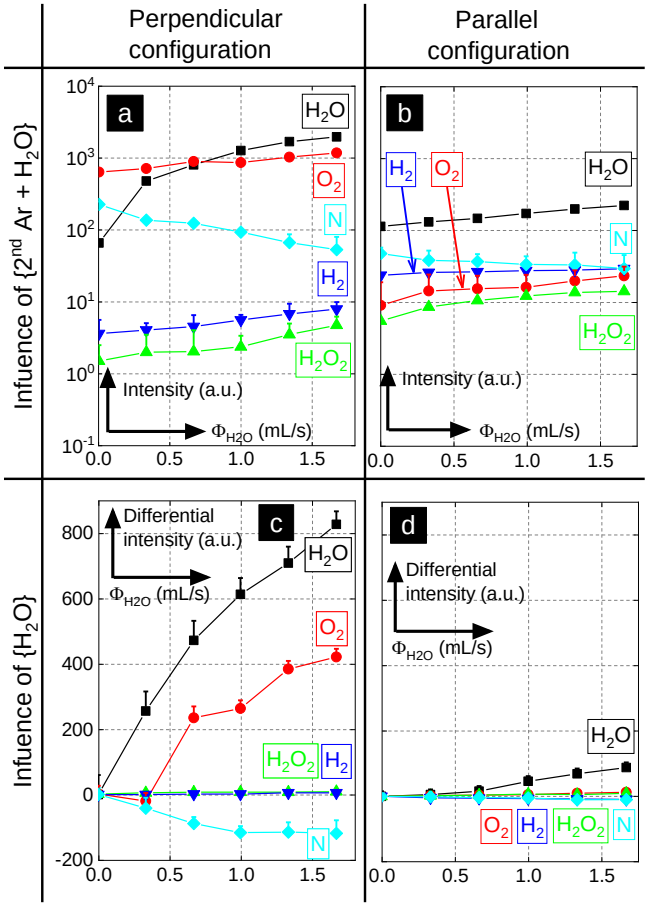


Figure 6. Mass spectrometry measurements showing the effect of the H_2O flow rate on the intensity and differential intensity of H_2O, O_2, H_2O_2, H_2 and N (Ar flow rate of 30 L min^{-1} and RF power of 80 W).

IV.2. Argon species in the post-discharge

The plasma torch is supplied in argon via two inputs: the first one allows striking and sustaining the discharge in the interelectrode region, while the second plays as a carrier gas for the water vapor in the inner post-discharge region. As shown in figures 4(a) and (b), a rise in the water vapor flow rate does not lead to a significant variation in the Ar emission, i.e. the excitation of Ar. However, the sole contribution of the water vapor, as highlighted in figures 4(c) and (d), shows a discrepancy in the emission of Ar: a decrease in the perpendicular configuration (outer region) with an increase in the parallel configuration (inner region). Similar behavior has been obtained with mass spectrometry, as shown in figures 5(c) and (d). Two possibilities may explain these patterns:

(i) the consumption of the Ar metastable species by the water vapor, as suggested by the reaction [R-11]. An increase in the H_2O reactant may consume more efficiently the Ar metastable species, thus resulting in one hand in the dissociation of H_2O into OH and H radicals as evidenced in the figure 4 and, on the other hand, in the excitation of Ar. As $\Phi(H_2O)$ increases, the emission of excited Ar species decays in the outer post-discharge due to the upwards consumption of the Ar^M which can no longer transfer part of their energy via [R-10]. As a result, the more water vapor is injected, the more the Ar species can be excited and confined in the inner post-discharge region.

(ii) injecting water vapor in the inner post-discharge may change the fluid dynamics of the main argon flow since it is injected perpendicularly. The resulting spatial distribution of the flow through the 126 holes grid would become more inhomogeneous by increasing the water vapor, i.e. becoming stronger through the holes located in the grid's central region and lower through the holes in periphery.

	#	Reaction	Rate constant
Inter-electrode region	[R-1]	$e + Ar \rightarrow e + Ar$	[a]
	[R-2]	$e + Ar \rightarrow e + Ar^*$	$k = 3.71\ 10^{-8}.\exp\left(-\frac{15.06}{T_e}\right)$
	[R-3]	$Ar^+ + Ar + e \rightarrow Ar^* + Ar$	$k = 1.01\ 10^{-11}$
	[R-4]	$Ar + e \rightarrow Ar^+ + 2e$	$k = 1.23\ 10^{-7}.\exp\left(-\frac{18.68}{T_e}\right)$
	[R-5]	$Ar^* + e \rightarrow Ar^+ + 2e$	$k = 2.05\ 10^{-7}.\exp\left(-\frac{4.95}{T_e}\right)$
	[R-6]	$Ar^* + Ar^* \rightarrow Ar^+ + e + Ar$	$k = 6.2\ 10^{-10}$
	[R-7]	$2Ar + Ar^+ \rightarrow Ar + Ar_2^+$	$k = 1.7\ 10^{-32}$
	[R-8]	$Ar + e \rightarrow Ar^M + e$	[a]
	[R-9]	$Ar + Ar^+ \rightarrow Ar^M + Ar^*$	[a]
Post-discharge region	[R-10]	$Ar^M + Ar \rightarrow Ar^* + Ar^*$	$k = 2.3\ 10^{-21}$
	[R-11]	$Ar^M + H_2O \rightarrow Ar + OH + H$	$k = 4.5\ 10^{-10}$
	[R-12]	$O(^1D) + H_2O \rightarrow OH + OH$	$k = 2.2\ 10^{-10}$
	[R-13]	$O(^3P) + H_2O \rightarrow OH + OH$	$k = 2.5\ 10^{-14}$
	[R-14]	$O + H + N_2 \rightarrow OH + N_2$	$k = 1.0\ 10^{-27}$
	[R-15]	$OH + OH + N_2 \rightarrow H_2O_2 + N_2$	$k = 1.6\ 10^{-23}$
	[R-16]	$H_2O + N_2^* \rightarrow H_2O + N_2$	$k = 3.9\ 10^{-10}$
	[R-17]	$O(^3P) + OH \rightarrow O_2 + H$	$k = 2.3\ 10^{-11}$
	[R-18]	$H_2O + O_3 \rightarrow H_2O_2 + O_2$	$k = 1.1\ 10^{-22}$
	[R-19]	$H + O_3 \rightarrow OH + O_2$	$k = 1.4\ 10^{-10}$
	[R-20]	$O_2 \rightarrow O + O$	$k = 1.01\ 10^{-8}$
	[R-21]	$OH + OH \rightarrow H_2O + O$	$k = 2.5\ 10^{-15}$
	[R-22]	$H_2O + O \rightarrow H_2O_2$	[a]

Table 2. Plausible reactions occurring in the Ar/H_2O post-discharge (units: $cm^3.s^{-1}$ for two-body collisions and $cm^6.s^{-1}$ for three-body collisions).

Simulations have been conducted by Atanasova et al on the current plasma torch for an argon flow rate set at 30 $L.min^{-1}$ [18]. They have revealed the existence of Ar_2^+ ions in the post-discharge, especially through dissociative recombination (see [R-7]) while no Ar^+ ion has been calculated. For instance, 2 mm away from the ground electrode, the density of Ar^+ is negligible while it is 5.10^{16} m^{-3} for Ar_2^+. As expected, Ar^+ ions has not been detected by OES. The Ar_2^+ ions have not been observed either due to the limited range of our optical spectrometer. Therefore, even if these ions could not be evidenced experimentally for material reasons, their existence in the first millimeter of the post-discharge is at least sustained by the simulations of Atanasova.

Two last observations on the OES and MS results are noteworthy:

(i) On the whole $\Phi(H_2O)$ range, the intensities of Ar are higher in figure 4(a) (approximately 8000 a.u.) than in figure 4(b) (approximately 1000 a.u.). The reason for this is that even if the optical fiber presents the same solid angle of collection independently of the configuration, the integration of the light depends on the configuration. As illustrated in figure 7, light is collected over 40 holes in the perpendicular configuration whereas approximately 8 holes in the parallel configuration. This explains also why the uncertainties on the data points are stronger in figure 4(b) than in figure 4(a).
(ii) The Ar mass spectra from figure 6 present similar trends of those obtained by OES. The intensities measured are however higher in the parallel configuration (see figure 6(b)) since the issue is no more dealing with a solid angle of collection but with the section of the capillary tube which collects more species when frontally exposed to the post-discharge flow.

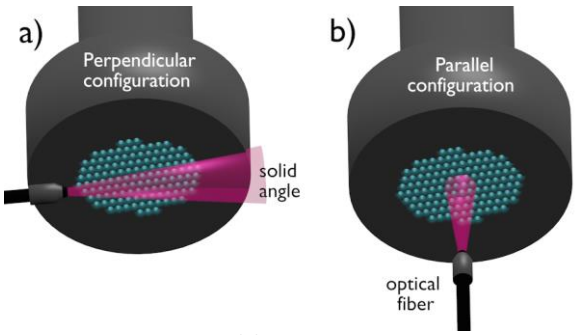


Figure 7. Regions analyzed in (a) the perpendicular configuration and (b) the parallel configuration.

IV.3. Electrons

The mean free path of an electron in the ambient air with an energy comprised between 20 and 100 eV is approximately 0.5 µm [24]. As in atmospheric post-discharges the electron temperature is usually lower than 2 eV [25], the corresponding mean free path is even much smaller than 0.5 µm. Owing to their very short mean free paths at atmospheric pressure, and to the thickness of the ground electrode (at least 1 mm), the presence of free electrons in the inner post-discharge region seems a priori highly hypothetical. However, the simulations of Atanasova et al conducted on this plasma torch indicate that, due to the effect of the flowing carrier gas, an electron density as low as 5.10^{10} cm^{-3} can be obtained 1 mm away from the ground electrode before it drastically drops to zero before reaching the grid [18]. Therefore, a very low electron density may be expected in the inner region of the post-discharge even if its role seems negligible for the excitation of Ar or the dissociation of H_2O owing to the too low energy of the electrons.

IV.4. H_2O molecules

Water vapor cannot be detected in the interelectrode region because of the configuration of the plasma torch. In the flowing post-discharge, two sources of water can be distinguished: the water vapor injected via the bubbler (source controlled) and the water vapor from the ambient air (source uncontrolled). The optical emission of H_2O molecules cannot be detected since occurring at 6260 nm [33] and 11876 nm [34]. However, mass spectrometry measurements revealed an increase in the intensity of H_2O with $\Phi(H_2O)$. As this increase is higher than when the plasma torch is off, it thus indicates a partial dissociation of the water vapor through at least one of the following reactions leading to the production of OH radicals, i.e. [R-11], [R-12] and [R-13].

IV.5. Nitrogen molecules

Both OES and MS measurements have evidenced the presence of molecular nitrogen in the post-discharge, due to the ambient air. In the perpendicular configuration, a gradual drop in the N_2 optical emission and MS peak intensity was observed as a function of the water vapor flow rate (see figures 4(c) and 5(c)). Molecular nitrogen can be deexcited by the dissociation products of H2O, i.e. OH and O, as previously stated through reactions [R-14] and [R-15]. Besides, MS measurements have evidenced a partial consumption of water in the discharge, meaning that N_2* might also be quenched by H_2O molecules ([R-16]). Reactions leading to the dissociation of N_2 or to the formation of N^+ ions are irrelevant since neither N nor N^+ emissions could be observed in the optical range. Furthermore, no optical emission of N_2^+ (15.58 eV) could be observed since Penning ionization of N_2 cannot be induced by the too-low energetic Ar^M species (11.55 eV) in the post-discharge [35–37].
In the parallel configuration, the drop of the N_2 emission (figure 5(c)) or N_2 MS intensity (figure 5(d)) only occurs when a tiny flow of water is injected (0.33 $mL.s^{-1}$). In our setup, a further increase in the water vapor flow rate remains too low to detect, by OES or MS, significant variations of N_2.

IV.6. OH radicals

For $\Phi(H_2O)$ = 0 $mL.s^{-1}$, the production of these OH radicals can result from the interaction of the post-discharge with the ambient atmosphere, where water vapor can be dissociated as shown by reaction [R-12], involving an excited oxygen radical as collisional partner. The production of OH radicals through electron impact processes in the post-discharge is highly hypothetical due to the too low energy and density of the electrons [38–40]. Moreover, the production of OH radicals in the interelectrode region is not expected since the plasma torch is supplied in argon and eventually in oxygen: no H source is present.
For $\Phi(H_2O)$ > 0 $mL.s^{-1}$, the production of OH can be understood combining the trends of OH and O emissions in figure 4(c) (perpendicular configuration). From 0 to 0.7 $mL.s^{-1}$, the consumption of atomic O is counterbalanced by the production of OH radicals, whereas beyond 0.7 $mL.s^{-1}$ an equilibrium seems to be reached for the consumption of O radicals; hence, there is a limitation in the emission of the OH radicals (around 1000 a.u.). As a result, the previous reaction [R-12] still occurs. Also, MS results in figure 5(c) indicate that at least one non-radiative process may also be responsible for their production since the intensity of OH increases as a function of the water vapor flow rate (while the emission of OH remains constant in figure 4(c)). As an example of this, the reaction [R-13] involving ground state oxygen atoms could be responsible for the production of non-emitting OH species.

S Collette, T Dufour, F Reniers, Plasma Sources Sci. Technol. 25 (2016) 025014, http://doi.org/10.1088/0963-0252/25/2/025014

IV.7. H radicals

The comparison between figures 4(c) and (d) shows that the production of H radicals through radiative processes has only been evidenced in parallel configuration; the mass spectrometry measurements indicate the production of H radicals both in ⊥ and // configurations (see figures 6(c) and (d)).
In the post-discharge, the injection of water vapor does not seem to favor the production of H radicals since no significant variation has been observed in the Hα emission in figure 4(d) and in its MS intensity in figure 5(d). However, variations can be observed in figures 4(b) and 5(b) where the influence of the secondary argon flow is taken into account, meaning that new pathways such as [R-11] and [R-17] may barely happen in the post-discharge. It is also worth mentioning that OES has not revealed any formation of molecular hydrogen since no Fulcher band could be detected between 590 nm and 640 nm irrespective of the setup configuration [41, 42]. The molecular hydrogen detected by MS (see figure 5) may result from the recombination of H atoms in the ionization chamber.

IV.8. O radicals and O_2 molecules

The production of O_2^+ ions has already been observed in the case of flowing post-discharges supplied in helium as a carrier gas [19]. These ions were the result of Penning ionization induced by He metastable species. Here, the Penning ionization of O_2 molecules by Ar metastable species can barely be suggested since no production of O_2^+ ions could be evidenced by OES. The reason for this is that the energetic level of Ar^M species is lower than the energy required to ionize O_2^+ ions. For the same reason, no O_2 metastable species could be evidenced since no band of the singlet sigma metastable oxygen $O_2(b^1\Sigma g^+)$ has been detected between 758 and 770 nm [19]. However, the presence of molecular oxygen has been highlighted by mass spectrometry as increasing with $\Phi(H_2O)$ irrespective of the configuration (see figure 6). Even without water injected, the figures 6(a) and (b) clearly indicate a peak intensity of O_2 specific to molecular oxygen from the ambient atmosphere. An increase in $\Phi(H_2O)$ is responsible for the production of O_2 through non-radiative processes such as [R-17], [R-18] and [R-19]. The ozone species required by the two latter reactions have already been measured in the outer post-discharge at concentrations comprised between 10^{14} and 10^{15} cm^{-3} by investigating the absorption of the mercury emission line [17].
One of the main pathways explaining the efficient production of atomic oxygen in the post-discharge is the direct dissociation of molecular oxygen contained in the ambient atmosphere (see [R-20]). However, another reaction—even if less obvious—should also be taken into account. Indeed, we have already stated that atomic oxygen could control the production of OH radicals essentially through reactions [R-12] and [R-13]. We have also noticed in figure 4(c) that any further increase in water vapor flow rate induced limitations of OH and O emissions. Those two plateaus may evidence an equilibrium with respect to the production/consumption of O and OH species, resulting from a reaction opposite to [R-12] and [R-13], namely [R-21]. In this reaction, two OH radicals could lead to the production of water and O radicals.

IV.9. H_2O_2

The formation of hydrogen peroxide was detected by mass spectrometry in the ⊥ and // configurations. Without injecting water vapor, a very tiny amount of H_2O_2 was detected and it may have resulted from [R-15] where two OH radicals in presence of molecular nitrogen leads to the production of H_2O_2. By injecting water vapor, two other reactions may enhance the mass spectrum intensity of H_2O_2 as shown in figures 6(a) and (b), namely reactions [R-18] and [R-22], with the first implying ozone molecules and the second one oxygen radicals.

IV.10. Stability

As shown in figure 1, the post-discharge stability is weakened as the water vapor flow rate is increased. The main reaction that could explain this trend is [R-11] where Ar metastable species are consumed by water. This consumption of Ar metastables can also be indirectly evidenced through the decrease in the post-discharge current versus the water vapor flow rate (see figure 3). Indeed, Bogaerts et al have shown that for a DC argon glow discharge, Ar_2^+ ions are predominantly formed by associative ionization, both through highly excited Ar** atoms (Hornback-Molar process) and by metastable-metastable collisions [43]. As [R-11] consumes the Ar metastable atoms, the Ar_2^+ ions can no longer be formed through this reaction, and so there is a partial decrease of the current intensity with $\Phi(H_2O)$.

V. Conclusion

The reactivity of water vapor introduced in the flowing post-discharge an atmospheric plasma torch was investigated firstly by correlating electrical characterization, OES and MS results and previous studies achieved with the same plasma source (one dealing with simulations and the other with experiments). Inhomogeneities were explained as resulting from the consumption of the Ar metastable species by H2O molecules. The gradual consumption in Ar_2^+ ions was advanced as an indirect consequence of this consumption in Ar metastables. Moreover, we have also shown the absence of any Penning ionization of O_2 and N_2 observed in a flowing helium post-discharge. The production and consumption reactions of O, OH and H radicals have been shown through various reactions, in particular the interdependency between O and OH. Finally, the interaction of the post-discharge with the ambient air has also been evidenced since molecular nitrogen was detected by OES.

VI. Acknowledgment

This work was part of the Interuniversity Attraction Pole (I.A.P) programs 'PSI _ Physical Chemistry of Plasma Surface Interactions—IAP-VII/12, P7/34—financially supported by the Belgian Federal Office for Science Policy (BELSPO).

VII. References

[1] Srivastava N and Wang C 2011 Effects of water addition on OH radical generation and plasma properties in an atmospheric argon microwave plasma jet J. Appl. Phys. 110 053304

[2] Magne L, Pasquiers S, Gadonna K, Jeanney P, Blin-Simiand N, Jorand F and Postel C 2009 OH kinetic in high-pressure plasmas of atmospheric gases containing C2 H6 studied by absolute measurement of the radical density in a pulsed homogeneous discharge J. Phys. D: Appl. Phys. 42 165203

[3] Koo I and Lee W 2004 Hydrogen isotope exchange reactions in an atmospheric pressure discharge utilizing water as carrier gas Plasma Chem. Plasma Process. 24 537–54

[4] Rybkin V, Kuvaldina E, Grinevich A, Choukourov A, Iwai H and Biederman H 2008 comparative study of poly(propylene) surface oxidation in DC low pressure oxygen and water vapor discharges and in flowing afterglow of water vapor discharge Plasma Process. Polym. 5 778–87

[5] Siow K S, Britcher L, Kumar S and Griesser H J 2006 Plasma methods for the generation of chemically reactive surfaces for biomolecule immobilization and cell colonization—a review Plasma Process. Polym. 3 392–418

[6] Fridman G, Friedman G, Gustol A, Shekhter A B, Vasilets V N and Fridman A 2008 Applied plasma medicine Plasma Process. Polym. 5 503–33

[7] Dufour T, Hubert J, Viville P, Duluard C, Desbief S, Lazzaroni R and Reniers F 2012 PTFE surface etching in the post-discharge of a scanning RF plasma torch: evidence of ejected fluorinated species Plasma Process. Polym. 9 820–9

[8] Dufour T, Minnebo J, Abou Rich S, Neyts E C, Bogaerts A and Reniers F 2014 Understanding polyethylene surface functionalization by an atmospheric He/O2 plasma through combined experiments and simulations J. Phys. D: Appl. Phys. 47 224007

[9] Abou Rich S, Leroy P, Dufour T, Wehbe N, Houssiau L and Reniers F 2014 In-depth diffusion of oxygen into LDPE exposed to an Ar-O2 atmospheric post-discharge: a complementary approach between AR-XPS and ToF-SIMS techniques Surf. Interface Anal. 46 164–74

[10] Sanchis M, Blanes V, Blanes M, Garcia D and Balart R 2006 Surface modification of low density polyethylene (LDPE) film by low pressure O2 plasma treatment Eur. Polym. J. 42 1558–68 [11] Zanolli Z, Leghrib R, Felten A, Pireaux J-J, Llobet E and Charlier J-C 2011 Gas sensing with Au-decorated carbon nanotubes ACS Nano 5

[12] Liu L, Xie D, Wu M, Yang X, Xu Z, Wang W, Bai X and Wang E 2012 Controlled oxidative functionalization of monolayer graphene by water–vapor plasma etching Carbon 50 3039–44

[13] Morra M, Occhiello E and Garbassi F 1993 The effect of plasma-deposited siloxane coatings on the barrier properties of HDPE J. Appl. Polym. Sci. 48 1331–40

[14] France R M and Short R D 1997 Plasma treatment of polymers effects of energy transfer from an argon plasma on the surface chemistry of poly(styrene), low density poly(ethylene), poly(propylene) and poly(ethylene terephthalate) J. Chem. Soc. Faraday Trans. 93 3173–8

[15] König U, Nitschke M, Menning A, Sperling C, Simon F, Arnhold C, Werner C and Jacobasch H-J 1999 Plasma modification of polytetrafluoroethylene for immobilization of the fibrinolytic protein urokinase Surf. Coat. Technol. 116 1011–5

[16] Zhang X, Li M, Zhou R, Feng K and Yang S 2008 Ablation of liver cancer cells in vitro by a plasma needle Appl. Phys. Lett. 93 021502

[17] Duluard C Y, Dufour T, Hubert J and Reniers F 2013 Influence of ambient air on the flowing afterglow of an atmospheric pressure Ar/O2 radiofrequency plasma J. Appl. Phys. 113 093303

[18] Atanasova M, Carbone E, Mihailova D, Benova E, Degrez G and van der Mullen J J 2012 Modelling of an RF plasma shower J. Phys. D: Appl. Phys. 45 145202

[19] Dufour T, Hubert J, Vandencasteele N and Reniers F 2012 Chemical mechanisms inducing a dc current measured in the flowing post-discharge of an RF He–O2 plasma torch Plasma Sources Sci. Technol. 21 045013

[20] Sarani A, Nikiforov A and Leys C 2010 Atmospheric pressure plasma jet in Ar and Ar/H2O mixtures: optical emission spectroscopy and temperature measurements Phys. Plasmas 17 063504

[21] Dony M, Ricard A, Dauchot J-P, Hecq M and Wautelet M 1995 Optical diagnostics of d.c. and r.f. argon magnetron discharges Surf. Coat. Technol. 75 479–84

[22] Zhao P, Lichten W, Layer H and Bergquist J C 1986 Remeasurement of the Rydberg constant Phys. Rev. A 34 5138–41

[23] Lee C and Lieberman M A 1995 Global model of Ar, O2, Cl2, and Ar/O2 high-density plasma discharges J. Vac. Sci. Technol. A 13 368

[24] Kazan B 1992 ADV Electronics Electron Physics vol 83 (New York: Academic) p 85

[25] Schutze A, Jeong J Y, Babayan S, Park J, Selwyn G S and Hicks F R 1998 The atmospheric pressure plasma jet: a review and comparison to other plasma sources IEEE Trans. Plasma Sci. 26 1685–94

[26] Hayashi M 1983 Determination of electron-xenon total excitation cross-section, from thereshold to 100 eV, from experimental values of Townsend's alphas J. Phys. D: Appl. Phys. 16 581

[27] Nafarizal N, Takada N and Sasaki K 2008 Production of Ar metastable atoms in the late afterglow of pulse-modulated rf magnetron sputtering plasmas J. Phys. D: Appl. Phys. 41 035206

[28] Bourene M, Dutuit O and Le Calve J 1975 De-excitation of the Ar 3P2, 3P1, and 1P1 states in pure argon and in Ar/H2 or Ar/CO mixtures J. Chem. Phys. 63 1668–75

[29] Shirafuji T and Murakami T 2015 Contribution of electrons, Ar(3P0,2), H2O+, and H3O+ to production of OH(A2Σ+) in a microdielectric barrier discharge of Ar/H2O Japan. J. Appl. Phys. 54 01AC03

[30] Pancheshnyi S V, Stariovskaia S M and Starikovskii A Y 2000 Collisional deactivation of N2(C, v = 0, 1, 2, 3) states by N2, O2, H2 and H2O molecules Chem. Phys. 262 349–57

[31] Hatakeyama S and Leu M-T 1989 Rate constants for reactions between atmospheric reservoir species J. Phys. Chem. A 93 5778–84

[32] Tsang W and Hampson R F 1986 Chemical kinetic data base for combustion chemistry. Part I. Methane and related compounds J. Phys. Chem. Ref. Data 15 1087

[33] Plyler E and Humphreys C 1948 Infrared emission spectra of flames J. Res. Natl Bur. Stand. 40 449–56

[34] Coheur P-F, Bernath P, Carleer M, Colin R, Polyansky O, Zobov N, Shirin S, Barber R and Tennyson J 2005 A 3000 K laboratory emission spectrum of water J. Chem. Phys. 122 074307
[35] Siders C, Rodriguez G, Siders J, Omenetto F and Taylor A 2001 Measurement of ultrafast ionization dynamics of gases by multipulse interferometric frequency-resolved optical gating Phys. Rev. Lett. 87 263002
[36] Lotito G, Nelis T, Guillot P and Günth D 2011 Characterization of argon metastable species as function of time, space, and current of a pulsed dc glow discharge Spectrochim. Acta B 66 619–26
[37] Velchev I, Hogervorst W and Ubachs W 1999 Precision VUV spectroscopy of Ar I at 105 nm J. Phys. B: At. Mol. Opt. Phys. 32 511–6
[38] Goree J, Liu B and Drake D 2006 Gas flow dependence for plasma-needle disinfection of S. mutans bacteria J. Phys. D: Appl. Phys. 39 3479–86
[39] Ono R and Oda T 2002 Dynamics and density estimation of hydroxyl radicals in a pulsed corona discharge J. Phys. D: Appl. Phys. 35 2133–8
[40] Khacef A, Cormier J M and Pouvesle J M 2002 NOx remediation in oxygen-rich exhaust gas using atmospheric pressure nonthermal plasma generated by a pulsed nanosecond dielectric barrier discharge J. Phys. D: Appl. Phys. 35 1491–8
[41] Xiao B, Kado S, Kajita S and Yamasaki D 2004 Rovibrational distribution determination of H2 in low temperature plasmas by Fulcher-α band spectroscopy Plasma Phys. Control. Fusion 46 653
[42] Yamasaki D, Kado S, Xiao B and Iida Y 2006 J. Phys. Soc. Japan 75 044501
[43] Bogaerts A and Gijbels R 1999 Role of Ar2+ and Ar2+ in a direct current argon glow discharge: a numerical description J. Appl. Phys. 86 4124–33